*Progress In Electromagnetics Research, Vol. 156, 25–35, 2016*

# Ferrite Magnetic-Anisotropy Field Effects on Inductance and Quality Factor of Planar GHz Inductors

**Jaejin Lee[1, 2], Yang-Ki Hong[2, *], Changhan Yun[3], Woncheol Lee[2], Jihoon Park[2], and Seok Bae[4]**

**Abstract**—Planar gigahertz (GHz) inductors were fabricated based on high crystalline-anisotropy $Zn_{0.13}Co_{0.04}Ni_{0.63}Fe_{2.2}O_4$ (Zn-Co-Ni ferrite) and $Ba_3Co_2Fe_{24}O_{41}$ ($Co_2Z$ hexaferrite) and characterized for inductance ($L$) and quality ($Q$) factor. The planar ferrite inductors show an $L$ of 4.5 nH (Zn-Co-Ni), 5.6 nH (Zn-Co-Ni + low $H_k$ and $f_{FMR}$ $Co_2Z$:), and 4.8 nH (Zn-Co-Ni + high $H_k$ and $f_{FMR}$ $Co_2Z$:) at 2 GHz. The corresponding $L$-densities are 18.0, 22.4, and 19.2 nH/mm$^2$, which are greater than 16.8 nH/mm$^2$ of the air-core inductor. With respect to the $Q$ factor, the air-core and ferrite inductors exhibit $Q$ factors of 6.7 (air-core), 4.8 (Zn-Co-Ni), 2.8 (Zn-Co-Ni + low $H_k$ $Co_2Z$), and 4.0 (Zn-Co-Ni + high $H_k$ $Co_2Z$) at 2 GHz. The $\tan\delta_\mu$ of the ferrites caused a reduction in the $Q$ factor. Nevertheless, the high $H_k$ and $f_{FMR}$ $Co_2Z$ ferrite inductor demonstrates a higher $Q$ factor than that of the low $H_k$ and $f_{FMR}$ $Co_2Z$ inductor. It is, therefore, suggested that high resistivity, anisotropy, magnetization ferrite can produce large $L$ density and $Q$ factor GHz inductors.

## 1. INTRODUCTION

Radio frequency (RF) transceivers with fully integrated circuits, including voltage controlled oscillators, low-noise amplifiers, and frequency filters, are in high demand for mobile electronic devices. In response to this, a large number of inductors are integrated into RF integrated circuits (RFICs). However, the inductors consume a large area of the RFICs, and their quality ($Q$) factors are critical for power management and RF signal processing. Therefore, compact and high $Q$ integrated inductors are required.

Integrated magnetic inductors have been widely investigated. A high-permeability material increases the $L$ and $Q$ factor of inductors by increasing magnetic flux density and decreasing coil resistance and parasitic capacitance [1, 2]. A 2 µm thick CoZrTa magnetic film inductor with relative permeability ($\mu_r$) of about 1000 showed a high $L$ density of 1.3 µH/mm$^2$ and a 28 times increase in $L$ compared to that of the air-core inductor [2]. However, low resistivity ($\rho = 99\,\mu\Omega\cdot$cm) of the CoZrTa film decreased the $Q$ factor below 6 at 1 GHz.

In an effort to address the low $Q$ factor, multilayered magnetic films [3–5] or high-resistivity ferrites ($\rho > 1\,k\Omega\cdot$cm) [6–9] were used in integrated inductors to suppress GHz eddy current loss. A FeGaB/$Al_2O_3$ multilayer solenoid inductor showed an $L$-density of 15 nH/mm$^2$ and $Q$ factor of 14 at 1.2 GHz [4]. A $Ni_{0.4}Zn_{0.4}Cu_{0.2}Fe_2O_4$ (Ni-Zn-Cu) ferrite spiral inductor had an $L$-density of 12 nH/mm$^2$ ($L$ of 1.94 nH) and $Q$ factor of 17.2 at 4 GHz, which were increases of about 3.9% and 6.3%, respectively, compared to those of the air-core inductor [9]. It is found that the high-resistivity ferrite is effective in increasing both $L$ and $Q$ factor at GHz frequencies [9, 10]. The $L$ of the ferrite inductor is enhanced by

*Received 9 February 2016, Accepted 10 April 2016, Scheduled 26 April 2016*

* Corresponding author: Yang-Ki Hong (ykhong@eng.ua.edu).

[1] Client Research and Development, Intel Corporation, Hillsboro, Oregon 97124, USA. [2] Department of Electrical and Computer Engineering, The University of Alabama, Tuscaloosa, AL 35487, USA. [3] Qualcomm Technologies, Inc., San Diego, CA 92121, USA. [4] LG Innotek Company Ltd., Ansan-si, Gyenggi-do 426-791, South Korea.

the ferrite's magnetic permeability ($\mu_r > 1$). The magnetic loss tangent ($\tan\delta_\mu$) of the ferrite plays a role and causes a decrease in GHz $Q$ factor.

The $Q$ factor of the ferrite inductor can be expressed by the air-core and magnetic-core components in Eq. (1) [13],

$$Q = \frac{\omega L}{R} = \frac{\omega L}{(R_{\mathrm{AC}} + \Delta R)}. \tag{1}$$

The resistance ($R_{\mathrm{AC}}$) of the air-core inductor is mainly attributed to conductor loss from skin-depth effect. The magnetic-core loss ($\Delta R \propto \tan\delta_\mu$) is related to the frequency-dependent loss $\tan\delta_\mu$. The $\tan\delta_\mu$ increases with frequency and becomes considerably large when the operating frequency approaches the ferromagnetic resonance frequency ($f_{FMR}$) of the ferrite. Therefore, a high $f_{FMR}$ ferrite is required, thereby contributing to low-loss characteristics and realizing high $Q$ GHz inductors. According to Eq. (2) [11]

$$f_{FMR} = (\gamma/2\pi)\sqrt{(4\pi M_s H_k)}, \tag{2}$$

$f_{FMR}$ increases with increasing $H_k$, where $H_k$ is the magneto-crystalline anisotropy field, $M_s$ the saturation magnetization, and $\gamma/2\pi$ the gyromagnetic constant (2.8 MHz/Oe). In contrast, ferrite's $\mu_r$ decreases with increasing $f_{FMR}$ by the Snoek law in Eq. (3) [12]

$$(\mu_r - 1)\cdot f_{FMR} = \frac{4}{3}\gamma M_s, \tag{3}$$

and $L$ consequently decreases. Therefore, a high crystalline-anisotropy ferrite inductor needs to be designed in consideration of magnetic parameters, including $H_k$, $M_s$, $\mu_r$, $f_{FMR}$, and $\tan\delta_\mu$.

In this paper, we investigate the relation of $H_k$ to inductor $Q$ factor and report electrical characteristics of high crystalline-anisotropy $Zn_{0.13}Co_{0.04}Ni_{0.63}Fe_{2.2}O_4$ (Zn-Co-Ni ferrite) and $Ba_3Co_2Fe_{24}O_{41}$ ($Co_2Z$ hexaferrite) inductors in comparison to an air-core inductor.

## 2. FUNDAMENTALS OF FERRITE INDUCTOR

### 2.1. Inductance and Quality Factor of a Ferrite Inductor

The $L$ of the ferrite inductor can be given by the sum of the air-core inductance ($L_{\mathrm{AC}}$) and the inductance gain ($\Delta L$) from the high-permeability ferrite in Eq. (4) [13],

$$L = L_{\mathrm{AC}} + \Delta L. \tag{4}$$

$L_{\mathrm{AC}}$ depends primarily on the geometry of a coil structure, including the length, width, and thickness. On the other hand, the gain $\Delta L$ is proportional to magnetic properties and geometry parameters of the ferrite in Eq. (5) [14, 15],

$$\Delta L \approx \mu_0 \mu_{eff} \frac{t_m w_m}{2 l_m}, \tag{5}$$

where

$$\mu_{eff} = \frac{\mu_r}{1 + N_d(\mu_r - 1)},$$

$t_m$, $w_m$, and $l_m$ are the thickness, width, and length of the ferrite, and $N_d$ is the demagnetization factor. Accordingly, the $L$ of the ferrite inductor can be enhanced by the ferrite's magnetic permeability ($\mu_r > 1$) as compared to the air-core ($\mu_r = 1$) inductor.

The $Q$ factor of the ferrite inductor is a function of the alternating current (AC) conductor loss ($R_{\mathrm{AC}}$) and magnetic-core loss ($\Delta R \propto \tan\delta_\mu$) according to Eq. (1). The $R_{\mathrm{AC}}$ can be reduced by the design optimization of inductor coil thickness, width, and length. With respect to the magnetic-core loss, the loss $\tan\delta_\mu$ is expressed by three main contributions in Eq. (6) [16],

$$\tan\delta_\mu = \tan\delta_h + \tan\delta_e + \tan\delta_r, \tag{6}$$

where $\tan\delta_h$ is the hysteresis loss, $\tan\delta_e$ the eddy current loss, and $\tan\delta_r$ the residual loss. For high-resistivity, soft-magnetic ferrites, the $\tan\delta_h$ and $\tan\delta_e$ become neligible. However, the $\tan\delta_r$, which is determined by the domain wall and spin rotational resonances, is predominant [17, 18]. For high $Q$ ferrite inductors, the $\tan\delta_\mu$ associated with the residual loss needs to be minimized.

### 2.2. Permeability Dispersion and Magnetic Loss of Ferrite

Permeability dispersion of a polycrystalline ferrite is associated with the domain wall motion and spin rotation, as given by Eqs. (7) and (8) [19]

$$\mu' = 1 + \frac{K_{DW}\omega_{DW}^2\left(\omega_{DW}^2 - \omega^2\right)}{\left(\omega_{DW}^2 - \omega^2\right)^2 + \beta^2\omega^2} + \frac{K_{sp}\omega_{sp}^2}{\omega_{sp}^2 + \omega^2}, \tag{7}$$

$$\mu'' = \frac{K_{DW}\omega_{DW}^2\beta\omega}{\left(\omega_{DW}^2 - \omega^2\right)^2 + \beta^2\omega^2} + \frac{K_{sp}\omega\omega_{sp}}{\omega_{sp}^2 + \omega^2}, \tag{8}$$

where $K_{DW}$ is the static magnetic susceptibility, $\omega_{DW}(= 2\pi f_{DW})$ the resonance frequency, $\beta$ the damping factor of the domain wall motion, $K_{sp}$ the static magnetic susceptibility, and $\omega_{sp}(= 2\pi f_{sp})$ the resonance frequency of the spin rotation. Based on the above equations, the individual loss components (i.e., $\tan\delta_{DW}$ and $\tan\delta_{sp}$) of the ferrite can be obtained by Eqs. (9) and (10), respectively.

$$\tan\delta_{DW} = \left(\frac{K_{DW}\omega_{DW}^2\beta\omega}{\left(\omega_{DW}^2 - \omega^2\right)^2 + \beta^2\omega^2}\right) \Big/ \left(\frac{K_{DW}\omega_{DW}^2\left(\omega_{DW}^2 - \omega^2\right)}{\left(\omega_{DW}^2 - \omega^2\right)^2 + \beta^2\omega^2}\right) = \frac{\beta\omega}{\omega_{DW}^2 - \omega^2}. \tag{9}$$

$$\tan\delta_{sp} = \left(\frac{K_{sp}\omega\omega_{sp}}{\omega_{sp}^2 + \omega^2}\right) / \left(\frac{K_{sp}\omega_{sp}^2}{\omega_{sp}^2 + \omega^2}\right) = \frac{\omega}{\omega_{sp}}. \tag{10}$$

It is noted that both the loss $\tan\delta_{DW}$ and $\tan\delta_{sp}$ decrease with increasing the resonance frequencies, $\omega_{DW}$ and $\omega_{sp}$. It is known that the domain wall resonance contributes to low-frequency permeability dispersion, while the spin rotational resonance is dominant in high-frequency permeability dispersion [20]. The high-frequency resonance frequency of ferrite, which is referred to as $f_{FMR}$, can be increased with high $H_k$ according to Eq. (2). Therefore, high resistivity, crystalline-anisotropy ferrite is necessary for high $L$-density and $Q$-factor GHz inductors.

## 3. EXPERIMENT

### 3.1. Inductor Design and Fabrication

A one-turn spiral inductor was designed as shown in Fig. 1(a). The inductor has a coil area of $0.5 \times 0.5\,\text{mm}^2$, width of 15 µm, space of 50 µm, and thickness of 7 µm. A bonding wire was used between the center and outermost pads for an electrical connection. This designed coil structure was

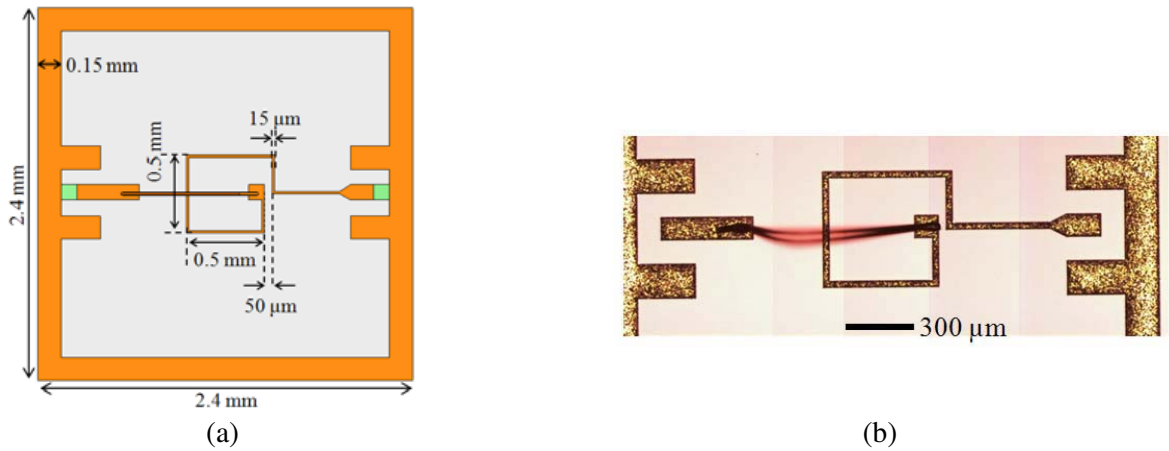


**Figure 1.** (a) Designed one-turn spiral inductor and (b) optical microscope image of the fabricated air-core inductor.

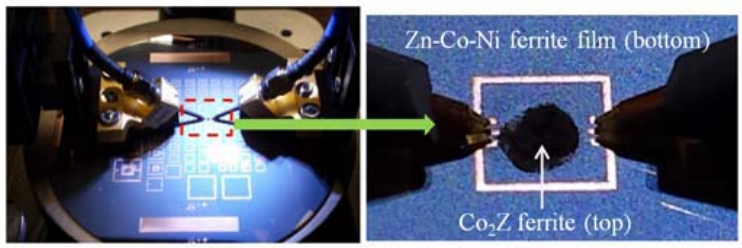


(a)

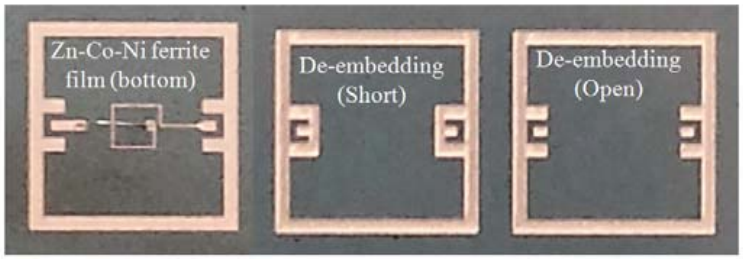


(b) (c) (d)

**Figure 2.** Photo-images of (a) embedded-type $Co_2Z$ hexaferrite inductor (bottom Zn-Co-Ni ferrite film + top $Co_2Z$ ferrite particles), (b) bottom-type Zn-Co-Ni ferrite film inductor, and (c) short and (d) open de-embedding structures.

used in simulating inductor performance (using ANSYS HFSS ver. 11) and fabricating air-core and ferrite inductors.

Figure 1(b) shows the air-core inductor that was fabricated on a 0.6 μm thick silicon oxide ($SiO_2$)/600 μm thick Si substrate. The conductivity ($\sigma$) of the Si substrate is 10–100 S/m. Figs. 2(a) and (b) exhibit the fabricated ferrite inductors with two different structures. One is the embedded-type ferrite inductor, where the inductor coil is positioned between the bottom Zn-Co-Ni ferrite film and top $Co_2Z$ hexaferrite particles as shown in Fig. 2(a). The second is the bottom-type ferrite inductor, having the coil formed on the Zn-Co-Ni ferrite film as presented in Fig. 2(b).

To fabricate the inductors, a microfabrication process and sputtering deposition were employed. First, a 2.45 μm thick Zn-Co-Ni ferrite film was deposited on the $SiO_2$/Si substrate, followed by Au (50 nm)/Ti (20 nm) seed layers for use in copper (Cu) coil electroplating. A 10 μm thick photoresist (PR) mold (Microchem KMPR1005) was then photolithographically produced on the Au/Ti layers. A 7 μm thick Cu coil was subsequently deposited by electroplating, followed by PR stripping and ion beam etching (IBE) of the Au/Ti layers for the bottom-type ferrite inductor as shown in Fig. 2(b). A mixture of $Co_2Z$ hexaferrite particles and ethanol was applied on the top of the bottom-type ferrite inductor and dried in air to realize the embedded-type ferrite inductor as presented in Fig. 2(a).

### 3.2. Preparation of High Crystalline-Anisotropy Zn-Co-Ni Ferrite Film and $Co_2Z$ Hexaferrite Particles

The Zn-Co-Ni ferrite film was prepared by the sequential direct current (DC) magnetron sputtering of nickel (Ni), iron (Fe), zinc (Zn), and cobalt (Co) metal targets in a mixture of 75% Ar and 25% $O_2$. During the sputtering deposition, the substrate temperature was held at 850°C, and the working pressure and DC power for each target were 5 mTorr and 250 W (200 W for Zn), respectively. The deposited multilayered oxide films were post-annealed at 850°C for 4 hours in a mixture of 67% Ar and 33% $O_2$ in order to crystallize the films into the Zn-Co-Ni ferrite.

With regard to $Co_2Z$ hexaferrite particles, the solid-state reaction process was used. The detailed process is reported elsewhere [21, 22]. Two different-sized $Co_2Z$ particles were prepared with and without 10-hour ball milling for the embedded-type ferrite inductor.

### 3.3. Measurement

The static magnetic properties and crystalline phases of the Zn-Co-Ni ferrite film and $Co_2Z$ particles were characterized by a vibrating sample magnetometer (MicroSense EV9) and X-ray diffractometer, respectively. A scanning electron microscope (SEM: JEOL 7000) was used to observe the cross-sectional image of the Zn-Co-Ni ferrite film.

To measure inductor electrical characteristics, a vector network analyzer (Agilent N5260A) and GSG probes (Cascade Microtech ACP40-GSG-200) were used. The $L$ and $Q$ factor of the air-core and ferrite inductors were calculated from the measured complex two-port scattering ($S$)-parameters ($S_{11}$, $S_{12}$, $S_{21}$, and $S_{22}$) [23]. The experimental setup for the inductor measurement is shown in Fig. 2(a). The probes were calibrated using the short-open-load-through (SOLT) technique with an impedance standard substrate (Cascade Microtech 101-190). The de-embedding technique [24] was also used to eliminate the parasitic effects of the probe pads and ground structure. The short and open de-embedding structures are shown in Figs. 2(c) and (d), respectively.

## 4. RESULTS AND DISCUSSION

### 4.1. Properties of High Crystalline-Anisotropy Zn-Co-Ni Ferrite Film and $Co_2Z$ Hexaferrite Particles

The measured X-ray diffraction patterns confirm that the Zn-Co-Ni ferrite film (in Fig. 3) and $Co_2Z$ particles (not shown here) are well crystallized into spinel and hexagonal ferrites, respectively. The cross-sectional SEM image in Fig. 4 shows that the Zn-Co-Ni ferrite film has a thickness of 2.45 μm and a smooth and clean surface.

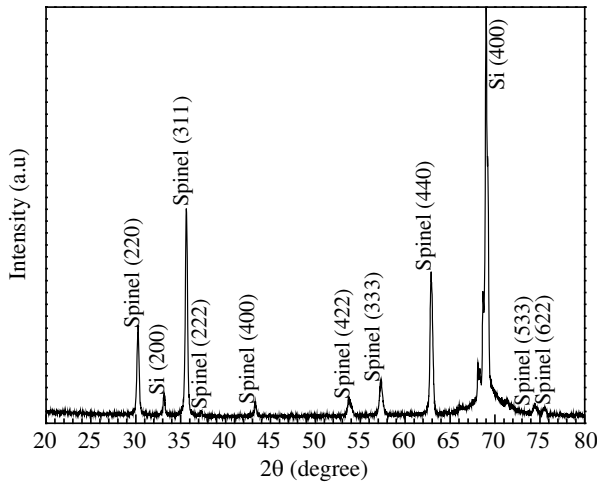


**Figure 3.** X-ray diffraction pattern of the fabricated Zn-Co-Ni ferrite film on silicon substrate.

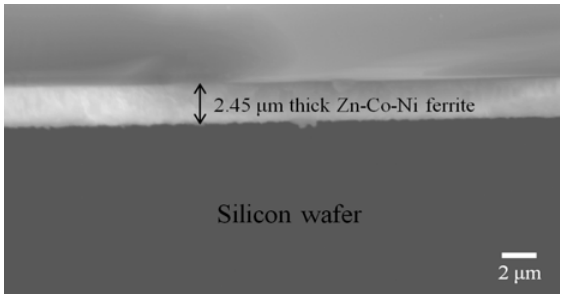


**Figure 4.** Scanning electron microscope (SEM) cross-sectional image of the Zn-Co-Ni ferrite film.

Figure 5 shows the measured magnetic hysteresis loop of the Zn-Co-Ni ferrite film. The saturation magnetization ($M_s$) and coercivity ($H_c$) of the film are 334 emu/cm$^3$ and 178 Oe, respectively. The in-plane $H_k$ of the ferrite film is 420 Oe, which was obtained by the method in [25]. It is noted that the fabricated Zn-Co-Ni ferrite film has higher $M_s$ and $H_k$ than those of low crystalline-anisotropy Ni-Zn-Cu ($M_s$ = 204 emu/cm$^3$, $H_k$ = 401 Oe) and YIG ($M_s$ = 94 emu/cm$^3$, $H_k$ = 238 Oe) ferrites [9]. It is, therefore, expected that the $f_{FMR}$ of the Zn-Co-Ni ferrite film increases with high $M_s$ and $H_k$ according to the relation $f_{FMR} = (\gamma/2\pi)(4\pi M_s H_k)^{0.5}$.

The measured magnetic hysteresis loops for the two different-sized $Co_2Z$ hexaferrites are presented in Fig. 6. One is the non-milled $Co_2Z$, while the other is the 10-hour milled $Co_2Z$ particles. The 10-hour milled $Co_2Z$ particles exhibit saturation magnetization ($\sigma_s$) of 49 emu/g and $H_c$ of 168 Oe. On the other

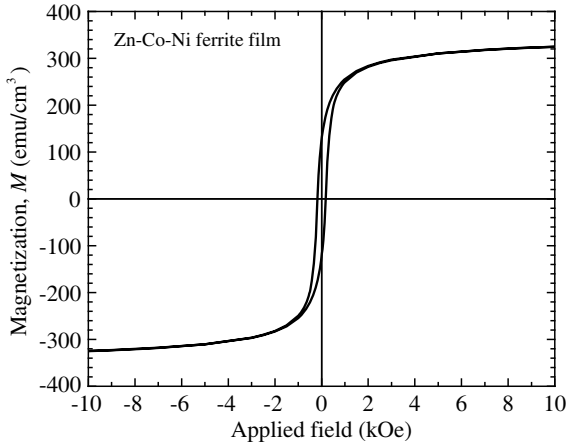


**Figure 5.** Measured magnetic hysteresis loop of the Zn-Co-Ni ferrite film.

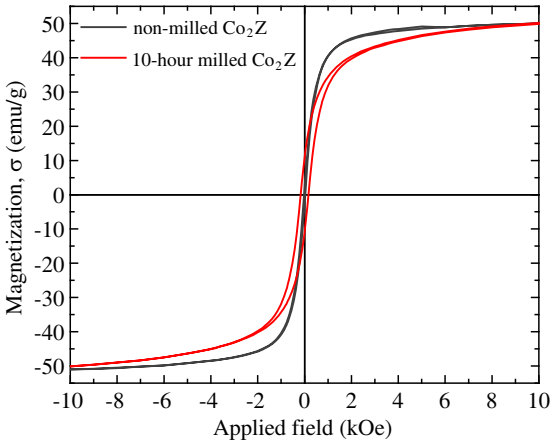


**Figure 6.** Measured magnetic hysteresis loops of the non-milled and 10-hour milled $Co_2Z$ hexaferrite particles.

hand, the non-milled $Co_2Z$ particles show $\sigma_s$ of 50 emu/g and $H_c$ of 23 Oe. The larger $H_c$ of the milled $Co_2Z$ implies a higher $H_k$ than that of the non-milled $Co_2Z$ [21].

With respect to dynamic magnetic properties, we calculated the frequency-dependent complex permeability for the Zn-Co-Ni ferrite film using Eq. (11) and permeability spectra for the $Co_2Z$ hexaferrite particles in order to estimate $\mu_r$, $\tan\delta_\mu$, and $f_{FMR}$. The complex permeability of the ferrite film can be calculated by Eq. (11) [26],

$$\mu(\omega) = 1 + \frac{\gamma 4\pi M_s}{\gamma H_k + j\alpha\omega} \times \left[1 + \frac{\omega^2}{(\gamma H_k + \gamma 4\pi M_s + j\alpha\omega)(\gamma H_k + j\alpha\omega) - \omega^2}\right], \tag{11}$$

where $\omega$ is the angular driving frequency, $\gamma$ the gyromagnetic constant ($1.76 \times 10^7$ rad/Oe·s), and $\alpha$ the damping constant. Thus, the parameters in the calculation include the experimental $M_s$ of 334 emu/cm$^3$, in-plane $H_k$ of 420 Oe, and $\alpha$ of 0.05 [27]. The calculated complex permeability spectra are presented in Fig. 7. The real part of permeability ($\mu'$) is about 14 at 2 GHz. The loss tan $\delta_\mu$ (at 2 GHz) and $f_{FMR}$ are 0.11 and 3.86 GHz, respectively. The $f_{FMR}$ is determined by the maximum imaginary part of permeability ($\mu''$). It is noted that the large $H_k$ and $M_s$ of the Zn-Co-Ni ferrite film leads to a higher

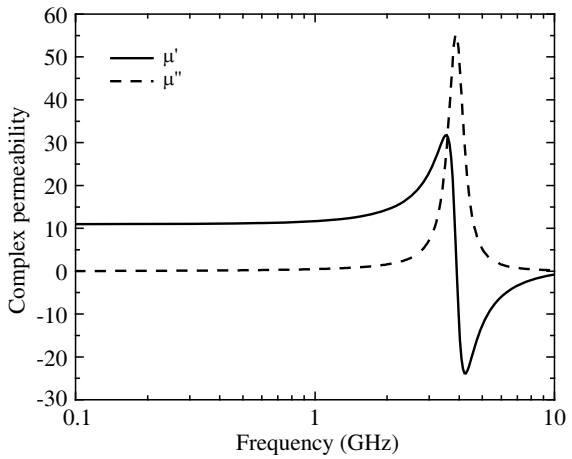


**Figure 7.** Calculated complex permeability of the Zn-Co-Ni ferrite film using the parameters $M_s = 334$ emu/cm$^3$, $H_k = 420$ Oe, and $\alpha = 0.05$.

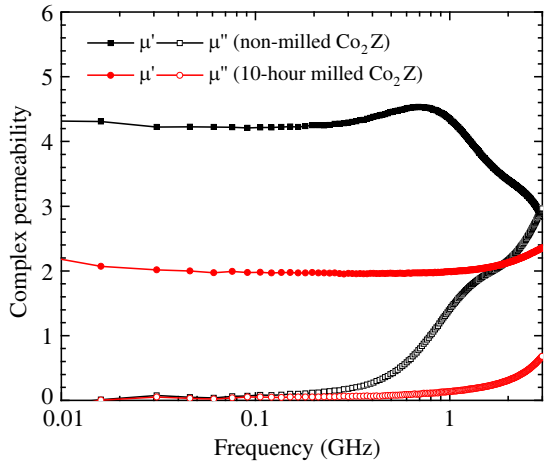


**Figure 8.** Measured complex permeability of the non-milled and 10-hour milled $Co_2Z$ hexaferrites.

$f_{FMR}$ than 0.26 GHz of the Ni-Zn-Cu ferrite and 0.06 GHz of the YIG [9]. The $\mu'$ and $\tan\delta_\mu$ were used in inductor performance simulation.

To measure the frequency-dependent complex permeability of the $Co_2Z$ hexaferrite, the $Co_2Z$ particles were formed into a toroidal ring (inner diameter: 3.2 mm, outer diameter: 7.8 mm) and characterized with an impedance/material analyzer (Agilent E4991). Fig. 8 presents the measured permeability spectra of the non-milled and 10-hour milled $Co_2Z$ hexaferrites. The $\mu'$ at 2 GHz is 3.4 (4.3 at 1 GHz) for the non-milled $Co_2Z$ and 2.1 (2.0 at 1 GHz) for the milled $Co_2Z$. The corresponding loss $\tan\delta_\mu$ are 0.64 (0.3 at 1 GHz) and 0.14 (0.06 at 1 GHz), respectively. It is obvious that the increased $H_k$ of the milled $Co_2Z$ leads to an increase in $f_{FMR}$ (beyond the measured frequency range in Fig. 8) and contributes to an improvement in GHz magnetic loss characteristics.

### 4.2. Electrical Characteristics of High Crystalline-anisotropy Zn-Co-Ni Ferrite Film Inductor

The fabricated ferrite inductors were characterized for $L$ and $Q$ factor in comparison to those of the air-core inductor. Figs. 9(a) and (b) show the measured and simulated $L$ and $Q$ factor of the bottom-type Zn-Co-Ni ferrite film and air-core inductors. The experimental $L$ and $Q$ factor of the inductors are in close agreement with the simulation results. It is noted that the discontinuity in the measured $Q$ factor in Fig. 9(b) is due to a minor measurement error. The measured $L$ of the Zn-Co-Ni ferrite and air-core inductors are 4.5 and 4.2 nH at 2 GHz, respectively. The corresponding $L$ densities are 18.0 and 16.8 nH/mm$^2$. It is found that the Zn-Co-Ni ferrite inductor shows a 7.1% increase in $L$ compared to that of the air-core inductor. The high crystalline-anisotropy Zn-Co-Ni ferrite inductor exhibits a small $L$ increase due to relatively low $\mu_r$.

With respect to the $Q$ factor of the inductors, the Zn-Co-Ni ferrite inductor shows a $Q$ factor of 4.8 at 2 GHz (8.5 at 1 GHz), which is lower than 6.7 (12.5 at 1 GHz) of the air-core inductor. The maximum $Q$ factors are 12.3 at 0.5 GHz for the Zn-Co-Ni ferrite and 14.1 at 0.55 GHz for the air-core inductors. The relatively low $Q$ factor of the ferrite inductor is mainly attributed to $\tan\delta_\mu$ of the Zn-Co-Ni ferrite. The measured inductor characteristics, therefore, indicate that GHz magnetic loss of the ferrite plays a critical role in inductor $Q$ factor. It is also found that the low $Q$ factors of both the air-core and Zn-Co-Ni ferrite inductors were caused by the large substrate loss of the high-conductivity Si substrate ($\sigma$ = 10–100 S/m). However, when we used the low-conductivity Si substrate ($\sigma$ = 0.01 S/m) in inductor performance simulation, the $Q$ factors of the Zn-Co-Ni ferrite and air-core inductors significantly increased to 20.0 and 31.9 at 2 GHz, respectively. The simulation results suggest that the Zn-Co-Ni ferrite film with high $M_s$ of 334 emu/cm$^3$ and $H_k$ of 420 Oe can produce an improved $L$-density, $Q$-factor inductor as compared to the low anisotropy Ni-Zn-Cu ferrite and YIG inductors [9].

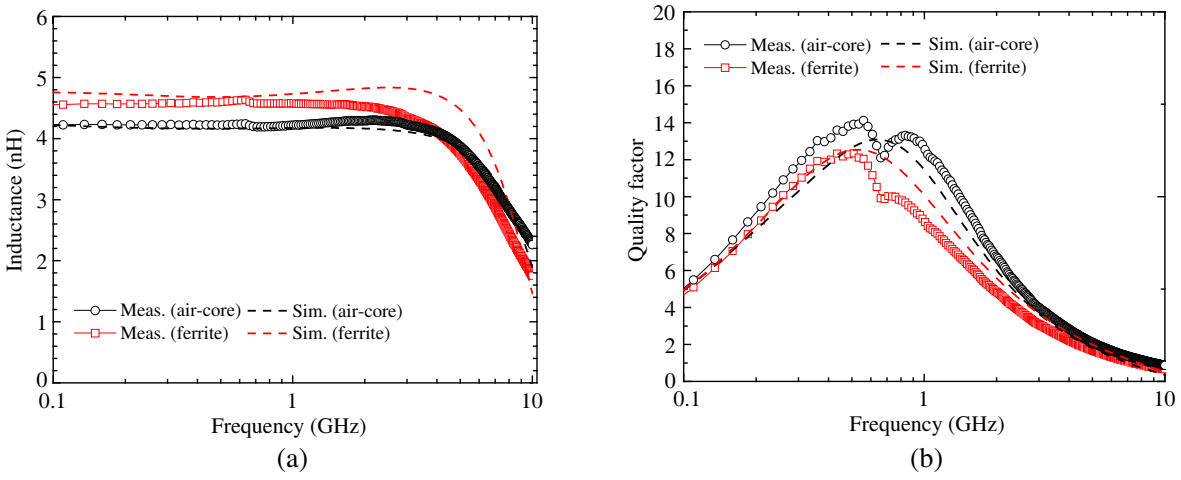


**Figure 9.** Measured and simulated (a) $L$ and (b) $Q$ factor of the air-core and Zn-Co-Ni ferrite film inductors.

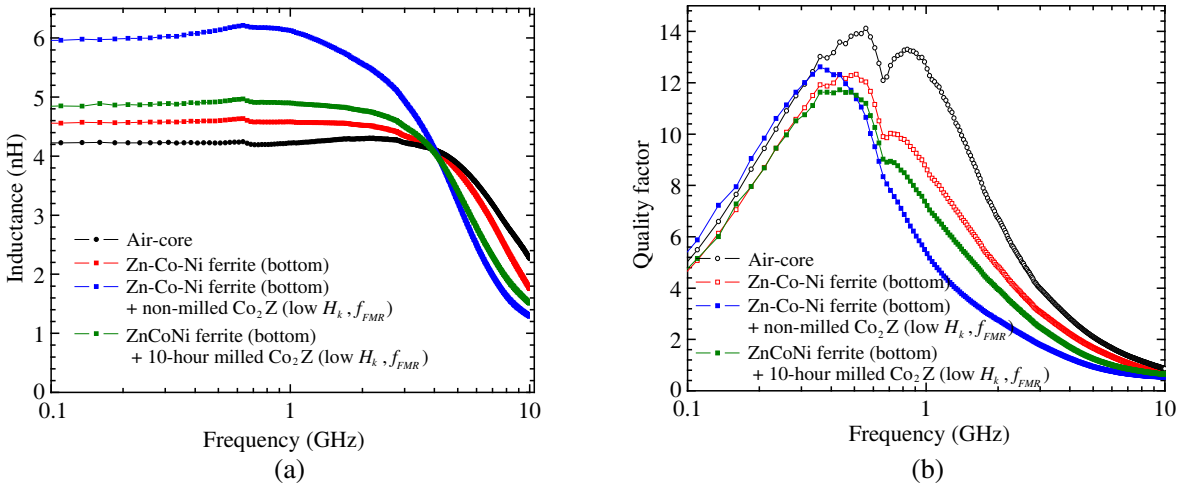


**Figure 10.** Measured (a) $L$ and (b) $Q$ factor of the air-core, Zn-Co-Ni ferrite (bottom), Zn-Co-Ni ferrite (bottom) + non-milled $Co_2Z$ hexaferrite (top), and Zn-Co-Ni ferrite (bottom) + 10-hour milled $Co_2Z$ hexaferrite (top) inductors.

**Table 1.** Measured electrical characteristics of the fabricated air-core and ferrite inductors at 2 GHz.

| At 2 GHz | $L$ (nH) | $L$ increase (%) | $Q$ | Max. $Q$ |
|---|---|---|---|---|
| Air-core | 4.2 | - | 6.7 | 14.1 at 0.55 GHz |
| Zn-Co-Ni ferrite film (bottom) | 4.5 | 7.1 | 4.8 | 12.3 at 0.50 GHz |
| Zn-Co-Ni ferrite film (bottom) + non-milled $Co_2Z$ (low $H_k$ and $f_{FMR}$) | 5.6 | 33.3 | 2.8 | 12.6 at 0.35 GHz |
| Zn-Co-Ni ferrite film (bottom) + 10 h-milled $Co_2Z$ (high $H_k$ and $f_{FMR}$) | 4.8 | 14.3 | 4.0 | 11.7 at 0.43 GHz |

### 4.3. Effect of Dynamic Magnetic Properties of $Co_2Z$ Hexaferrites on $L$ and $Q$ Factor

To further investigate the effect of dynamic magnetic properties on a ferrite inductor's $L$ and $Q$ factor, two-different sized $Co_2Z$ hexaferrites were applied to the bottom-type ferrite inductor as shown in Fig. 2(a). Fig. 10 shows the measured $L$ and $Q$ factor of the embedded-type ferrite inductors, with the coil positioned between the bottom Zn-Co-Ni ferrite film and top $Co_2Z$ hexaferrite particles, in comparison to the electrical characteristics of the air-core and bottom-type Zn-Co-Ni ferrite inductors. The embedded-type ferrite inductors show an $L$ of 5.6 nH (Zn-Co-Ni + non-milled $Co_2Z$: low $H_k$ and $f_{FMR}$) and 4.8 nH (Zn-Co-Ni + 10-hour milled $Co_2Z$: high $H_k$ and $f_{FMR}$) at 2 GHz. These inductances are greater than 4.2 nH of the air-core and 4.5 nH of the Zn-Co-Ni ferrite film inductors. The $L$ of the embedded-type ferrite inductors increase by 33% and 14% compared to the $L$ of the air-core inductor. The corresponding $L$-densities are 22.4 nH/mm$^2$ for the low $H_k$ $Co_2Z$ and 19.2 nH/mm$^2$ for the high $H_k$ $Co_2Z$. The significant increase in $L$ occurs because the $Co_2Z$ hexaferrite enhances magnetic flux density and also reduces leakage magnetic flux. On the other hand, the additional $\tan\delta_\mu$ from the $Co_2Z$ caused a reduction in the $Q$ factor as shown in Fig. 10(b). It is found that the high $H_k$ and $f_{FMR}$ $Co_2Z$ embedded-type inductor demonstrates a higher $Q$ factor of 4.0 at 2 GHz (7.2 at 1 GHz) than 2.8 (5.3 at 1 GHz) of the low $H_k$ and $f_{FMR}$ $Co_2Z$ inductor. Table 1 summarizes the measured characteristics of the fabricated air-core and ferrite inductors.

### 4.4. Relation of Magneto-Crystalline Anisotropy Field, $H_k$ to Inductor $Q$ Factor

The experimental inductor characteristics demonstrate that GH $\tan\delta_\mu$ plays a role in the inductor $Q$ factor, and therefore, the $H_k$ becomes a key magnetic parameter. Inductor performance simulation was

carried out to investigate the relation of $H_k$ to inductor $Q$ factor. Fig. 11 shows the dependence of both $f_{FMR}$ and $Q$ factor on $H_k$ at $\mu_{\rm dc}$ of 10, 20, and 30. The relation $\mu_{\rm dc} = 1 + 4\pi M_s/H_k$ and the Eqs. (2) and (11) were used to obtain the $f_{FMR}$ (in Fig. 11) and frequency-dependent $\mu'$ and $\tan\delta_\mu$. The calculated $\mu'$ and $\tan\delta_\mu$ at 2 GHz were then applied in the inductor simulation to determine the $Q$ factor. The designed inductor geometry shown in Fig. 1(a) was used. The Si-substrate had $\sigma$ of 0.01 S/m, and the ferrite film had a thickness of 2.45 µm. As shown in Fig. 11, the $f_{FMR}$ increases with increasing the $H_k$. At $\mu_{\rm dc}$ of 10, the $f_{FMR}$ increases to 5 GHz from less than 2 GHz as the $H_k$ increases from 200 to 600 Oe. The results suggest that the GHz $\tan\delta_\mu$ can decrease with high $H_k$ according to Section 2. The corresponding inductor $Q$ factor at 2 GHz is 37.9 with the $H_k$ of 600 Oe and 3.4 with the $H_k$ of 200 Oe. When the $H_k$ is higher than 400 Oe, the ferrite inductors' $Q$ factors become greater than that of the air-core inductor ($Q$ of 31.9 for the Si $\sigma$ of 0.01 S/m). With respect to the $L$, the simulated $L$ was about 4.4 nH at $\mu_{\rm dc}$ of 10, 4.6 nH at $\mu_{\rm dc}$ of 20, and 4.8 nH at $\mu_{\rm dc}$ of 30. It is, therefore, suggested that the high $H_k$ and $f_{FMR}$ ferrite inductor with a large $M_s$ is desired for high $L$ density and $Q$ factor GHz inductors.

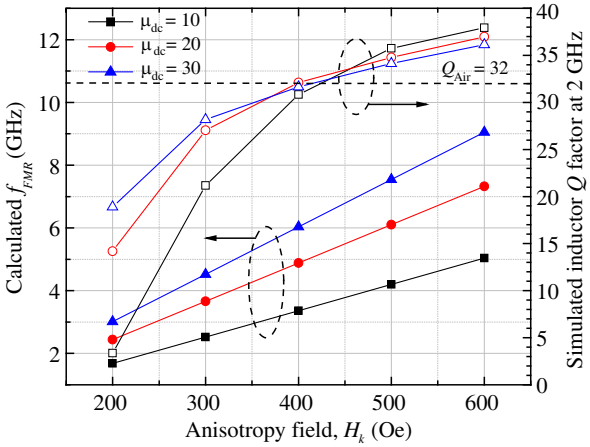


**Figure 11.** Calculated $f_{FMR}$ and simulated inductor $Q$ factor at 2 GHz as a function of $H_k$ at $\mu_{\rm dc}$ of 10, 20, and 30.

Exploring material candidates suggests that exchange-coupled magnets can meet the desired magnetic properties. The coupling of magnetically soft (i.e., high $M_s$ and small $H_k$) and hard (i.e., small $M_s$ and high $H_k$) phases in the exchange-coupled system realizes simultaneously high $M_s$ and large $H_k$. Therefore, future research will focus on exchange-coupled magnetic GHz inductors.

## 5. CONCLUSION

Planar GHz inductors were fabricated based on high crystalline-anisotropy Zn-Co-Ni ferrite and $Co_2Z$ hexaferrite and characterized for $L$ and $Q$ factor. The ferrite inductors show $L$ densities of 18.0 nH/mm$^2$ (Zn-Co-Ni), 22.4 nH/mm$^2$ (Zn-Co-Ni + low $H_k$ and $f_{FMR}$ $Co_2Z$:), and 19.2 nH/mm$^2$ (Zn-Co-Ni + high $H_k$ and $f_{FMR}$ $Co_2Z$:). With respect to the $Q$ factor, the ferrite inductors exhibit $Q$ factors of 4.8 (Zn-Co-Ni), 2.8 (Zn-Co-Ni + low $H_k$ $Co_2Z$), and 4.0 (Zn-Co-Ni + high $H_k$ $Co_2Z$) at 2 GHz. The $L$ densities and $Q$ factors of the ferrite inductors are greater and lower than 16.8 nH/mm$^2$ and 6.7 of the air-core inductor, respectively. The high $H_k$ of Zn-Co-Ni ferrite film and $Co_2Z$ hexaferrite results in increased $f_{FMR}$ and moderate $\mu_r$, but the ferrites' $\tan\delta_\mu$ causes a decrease in the $Q$ factor. Accordingly, $L$ densities and $Q$ factors are trade-off for GHz ferrite inductors. Future research needs to focus on development of low-loss and high-permeability GHz ferrites. In addition, low-temperature fabrication technique is inevitable since the ferrite process temperature is incompatible with complementary metal-oxide-semiconductor (CMOS) processing temperature in contrast to air-core inductors. In conclusion, the simulation and experiment results suggest that high resistivity, crystalline-anisotropy, low loss ferrite along with high $Q$ inductor design can give rise to high $L$ density and $Q$ factor GHz inductors.

## REFERENCES


1. Yamaguchi, M., M. Baba, and K. I. Arai, "Sandwich-type ferromagnetic RF integrated inductor," *IEEE Trans. Microwave Theory Tech.*, Vol. 49, No. 12, 2331–2335, 2001.
2. Gardner, D. S., G. Schorom, P. Hazucha, F. Paillet, T. Karnik, S. Borkar, R. Hallstein, T. Dambrauskas, C. Hill, C. Linde, W. Worwang, R. Baresel, and S. Muthukumar, "Integrated on-chip inductors using magnetic material," *J. Appl. Phys.*, Vol. 103, No. 7, 07E927-1–07E927-6, 2008.
3. Sato, N., Y. Endo, and M. Yamaguchi, "Skin effect suppression for Cu/CoZrNd multilayered inductor," *J. Appl. Phys.*, Vol. 111, No. 7, 07A501-1–07A501-3, 2012.
4. Gao, Y., S. Zare, X. J. Yang, T. X. Nan, Z. Y. Zhou, M. Onabajo, K. P. O'Brien, U. Jalan, M. El-tanani, P. Fisher, M. Liu, A. Aronow, K. Mahalingam, B. M. Howe, G. J. Brown, and N. X. Sun, "High quality factor integrated gigahertz magnetic transformers with FeGaB/$Al_2O_3$ multilayer films for radio frequency integrated circuits applications," *J. Appl. Phys.*, Vol. 115, No. 17, 17E714-1–17E714-3, 2014.
5. Davies, R. P., C. Cheng, N. Sturcken, W. E. Bailey, and K. L. Shepard, "Coupled inductors with crossed anisotropy CoZrTa/$SiO_2$ multilayer cores," *IEEE Trans. Magn.*, Vol. 49, No. 7, 4009–4012, 2013.
6. Kaneko, K., N. Inoue, N. Furutake, and Y. Hayashi, "A novel multilayered Ni-Zn-ferrite/TaN film for RF/mobile applications," *Jpn. J. Appl. Phys.*, Vol. 49, No. 4, 04DB15-1–04DB15-5, 2010.
7. Qu, W., X. H. Wang, and L. Li, "Preparation and performance of NiCuZn-$Co_2Z$ composite ferrite material," *J. Magn. Magn. Mater.*, Vol. 257, No. 2–3, 284–289, 2003.
8. Cai, H. L., J. Zhan, C. Yang, X. Chen, Y. Yang, B. Y. Chi, A. Wang, and T. L. Ren, "Application of ferrite nanomaterial in RF on-chip inductors," *J. Nanomater.*, Vol. 2013, 1–12, 2013.
9. Yang, C., F. Liu, X. Wang, J. Zhan, A. Wang, T. L. Ren, L. T. Liu, H. Long, Z. Wu, and X. Li, "Investigation of on-chip soft-ferrite-integrated inductors for RFICs — Part II: Experiments," *IEEE Trans. Electron Devices*, Vol. 56, No. 12, 3141–3148, 2009.
10. Cai, H. L., Y. Yang, N. Qi, X. Chen, H. Tian, Z. Song, Y. Xu, C. J. Zhou, J. Zhan, A. Wang, B. Chi, and T. L. Ren, "A 2.7-mW 1.36–1.86-GHz LC-VCO with a FOM of 202 dBc/Hz enabled by a 26%-size-reduced nano-particle-magnetic-enhanced inductor," *IEEE Trans. Microwave Theory Tech.*, Vol. 62, No. 5, 1221–1228, 2014.
11. Kittel, C., "On the theory of ferromagnetic resonance absorption," *Phys. Rev.*, Vol. 73, No. 2, 155–161, 1948.
12. Smit, J. and H. P. J. Wijn, *Ferrites*, 271, John Wiley & Sons, New York, 1959.
13. Lee, D. W., K. P. Hwang, and S. X. Wang, "Fabrication and analysis of high-performance integrated solenoid inductor with magnetic core," *IEEE Trans. Magn.*, Vol. 44, No. 11, 4089–4095, 2008.
14. Lee, D. W. and S. X. Wang, "Effects of geometries on permeability spectra of CoTaZr magnetic cores for high frequency applications," *J. Appl. Phys.*, Vol. 103, No. 7, 07E907-1–07E907-3, 2008.
15. Soohoo, R. F., "Magnetic thin film inductor for integrated circuit applications," *IEEE Trans. Magn.*, Vol. 15, No. 6, 1803–1805, 1979.
16. Moulson, J. and J. M. Herbert, *Electroceramics: Materials, Properties, Applications*, John Wiley & Sons, 2003.
17. Chikazumi, S., *Physics of Ferromagnetism*, John Wiley & Sons, 1964.
18. Stoppels, D., "Developments in soft magnetic power ferrites," *J. Magn. Mater.*, Vol. 160, No. 1, 323–328, 1996.
19. Tsutaoka, T., M. Ueshima, and T. Tokunaga, "Frequency dispersion and temperature variation of complex permeability of Ni-Zn ferrite composite materials," *J. Appl. Phys.*, Vol. 78, No. 6, 3983–3991, 1995.
20. Rado, G. T., R. W. Wright, and W. H. Emerson, "Ferromagnetism at very high frequencies. III. Two mechanisms of dispersion in a ferrite," *Phys. Rev.*, Vol. 80, No. 2, 273–280, 1950.

21. Lee, J., Y. K. Hong, S. Bae, J. Jalli, G. S. Abo, J. Park, W. M. Seong, S. H. Park, and W. K. Ahn, "Low loss $Co_2Z$ ($Ba_3Co_2Fe_{24}O_{41}$)-glass composite for gigahertz antenna application," *J. Appl. Phys.*, Vol. 109, No. 7, 07E530-1–07E530-3, 2011.
22. Bae, S., Y. K. Hong, J. J. Lee, J. Jalli, G. S. Abo, A. Lyle, I. T. Nam, W. M. Seong, J. S. Kim, and S. H. Park, "New synthetic route of Z-type ($Ba_3Co_2Fe_{24}O_{41}$) hexaferrite particles," *IEEE Trans. Magn.*, Vol. 45, No. 6, 2557–2560, 2009.
23. Yook, J. M., J. H. Ko, M. L. Ha, and Y. S. Kwon, "High-quality solenoid inductor using dielectric film for multichip modules," *IEEE Trans. Microwave Theory Tech.*, Vol. 53, No. 6, 2230–2234, 2005.
24. Lee, D. W., "Integrated inductor with magnetic core: A realistic option," Ph.D. dissertation, Stanford University, Stanford, CA, 2008.
25. Kondo, K., T. Chiba, H. Ono, S. Yoshida, Y. Shimada, N. Matsushita, and M. Abe, "Conducted noise suppression effect up to 3 GHz by NiZn ferrite film plated at 90°C directly onto printed circuit board," *J. Appl. Phys.*, Vol. 93, No. 10, 7130–7132, 2003.
26. Tanaka, T., Y. K. Hong, S. H. Gee, M. H. Park, D. W. Erickson, and C. Byun, "Analytical calculation for estimation of magnetic film properties for a 3-GHz thin film inductor," *IEEE Trans. Magn.*, Vol. 40, No. 4, 2005–2007, 2004.
27. Shen, X., R. Gong, Z. Feng, and Y. Nie, "Effective permeability of NiZnCo ferrite granular thin films," *J. Am. Ceram. Soc.*, Vol. 90, No. 7, 2196–2199, 2007.